Appl Phys A (2010) 99: 865–869
DOI 10.1007/s00339-010-5620-5

Applied Physics A
Materials Science & Processing

Photoluminescence and field-emission properties of Cu-doped SnO_2 nanobelts

L.J. Li · K. Yu · H.B. Mao · Z.Q. Zhu

Received: 5 October 2009 / Accepted: 8 March 2010 / Published online: 24 March 2010

Abstract By using a thermal evaporation and condensation method, Cu-doped SnO_2 nanobelts were synthesized on silicon substrate. High-resolution transmission electron microscopy and energy dispersive X-ray spectroscopy studies of Cu-doped SnO_2 nanobelts demonstrate that the nanobelts are single-crystal structures and Cu is homogeneously doped into the SnO_2 lattice. X-ray diffraction further confirmed the single-phase nature of these nanobelts. The photoluminescence measurements of the nanobelts and samples annealed in oxygen were measured from 77 K to 300 K. Field-emission measurements demonstrated that the Cu-doped nanobelts possessed good performance with a turn-on field of ∼2.9 V/μm and a threshold field of ∼4.8 V/μm.

1 Introduction

Since the first discovery of carbon nanotubes [1], there have been significant research efforts to study one-dimensional (1D) nanostructure semiconductors, such as nanotubes, nanowires, nanorods and nanobelts due to their novel properties [2–6]. As a wide band gap (3.6 eV of bulk material at room temperature) semiconductor with large exciton binding energy of 130 meV, SnO_2 is a promising material with many applications, such as chemical sensors [7], lithium ion electrode materials [8], solar cells [9], cathode emitters of the field-emission (FE) device [10], and so forth. Therefore, syntheses and optical properties of one-dimensional SnO_2 nanostructures have widely been reported.

L.J. Li · K. Yu (✉) · H.B. Mao · Z.Q. Zhu
Key Laboratory of Polar Materials and Devices (Ministry of Education of China), Department of Electronic Engineering, East China Normal University, Shanghai 200241, People's Republic of China
e-mail: yk5188@263.net

As is well known, doping in semiconductors with selective elements offers an effective approach to adjust the electrical, optical, and magnetic properties, which is crucial for practical applications [11–13]. Optical measurements are very useful to the determination of the structure, defects, and impurities in nanostructures. The photoluminescence properties of undoped and doped SnO_2 have been widely studied [14–16]. Studies on the luminescence of 1D SnO_2 nanostructures at room temperature have revealed emission in the range of 400 to 600 nm [17–20]. It has been generally believed that the luminescence originates from defects such as tin interstitials, dangling bonds, or oxygen vacancies. However, no further investigations have been made on the formation and optical properties of 1D Cu-doped SnO_2 nanobelts.

The field-emission (FE) properties of many 1D nanomaterials have been widely studied due to their high surface-to-volume and their special morphology. In the last few years, the FE measurement results of SnO_2 nanostructures such as nanobelts, nanowhiskers and beaklike nanorods [10, 21, 22] show that 1D and quasi-1D SnO_2 nanostructures have promising applications in the FE device. However, up to now there have been few reports on electron field emission from Cu-doped tin oxide nanobelts.

In this work, the Cu-doped SnO_2 nanobelts were synthesized by thermal evaporation and condensation method. The nanobelts are single-crystalline structures and without other secondary phases or clusters. The temperature dependence photoluminescence properties of the nanobelts and samples annealed in oxygen were studied in detail. The FE property of the as-prepared SnO_2 nanobelts was investigated for the first time.

2 Experiments details

The growth was performed using an Au catalyst deposited silicon substrates in a conventional horizontal hot-wall chemical vapor transport system at atmospheric pressure. For the synthesis of the Cu-doped SnO_2 nanobelts, a reactant mixture of SnO power and $CuCl_2$ (99.99%, in purity) was placed at the end of a long quartz boat. The substrates were placed at a distance away from source materials. The tube furnace was ramped to the desired temperature (900°C). After the temperature was reached and kept for a few minutes, the boat was placed inside the center of the horizontal tube furnace. High-purity argon (99.99%) gas (500 sccm) was introduced into the tube as the carrier gas, and the furnace had been heated at 900°C for 1.5 hours. After the furnace was cooled down to room temperature, a light white layer sample was found on the surface of the substrate.

3 Results and discussion

Figure 1(a) shows the transmission electron microscopy (TEM, JEM2010) image of as-fabricated samples having a belt shape with a width of 40–200 nm and a length of up to a few micrometers. The high-resolution (HR) TEM image of the nanobelts indicated by the oval in Fig. 1(a) is shown in Fig. 1(b), from which it can be seen that the nanobelts are of single-crystalline structure except a little dislocation parallel to the wire axis, without secondary phases or clusters. The selected area electron diffraction (SAED) pattern recorded on the belt [the inset of Fig. 1(b)] indicates that the nanobelts grow along the [101] direction. Combining the HRTEM image and SAED pattern, it can be measured that the d spacings are 0.267 and 0.237 nm, which nearly agree with the d spacings of (101) (0.264 nm) and (200) (0.236 nm) of the tetragonal SnO_2. Energy dispersive x-ray spectroscopy (EDS) analysis of the samples, shown in Fig. 1(c), reveals the presence of Sn, Cu and O. Measurements on more than 10 different nanowires from the same substrate were carried out, and the most doped nanobelts in this investigation have a copper concentration of $\sim 2 \pm 0.5\%$. No signals of other elements are observed except some Fe and Cr signals come from the used TEM grid. The x-ray diffraction pattern further confirmed the single-phase nature of these nanobelts.

The x-ray diffraction (XRD D/max 2550V) patterns of the undoped SnO_2 and Cu-doped SnO_2 nanobelts are compared in Fig. 2. The diffraction peaks of the undoped SnO_2 nanobelts exactly match those of the SnO_2 of a tetragonal rutile structure ($a = b = 0.4739$ nm and $c = 0.3186$ nm; JCPDS Card No. 77-0448). The Cu-doped SnO_2 nanobelts have a highly crystalline structure with no evidence of other copper oxide or metal copper phases within the sensitivity of XRD measurements. From Fig. 2, it was found that the Cu doping shifts all the peak positions to lower angles relative to those of the undoped SnO_2 nanobelts. For instance, the dominant (110), (101), and (200) peaks of the Cu-doped SnO_2 nanobelts are shifted to a lower angle by 0.094°, 0.085° and 0.079° respectively, indicating the expansion of lattice constants of the Cu-doped SnO_2 crystal as the result of TEM. The unit cell parameters are $a = b = 0.4756$ nm and $c = 0.3188$ nm. This lattice expansion may be attributed to the substitution of the larger Cu^{2+} ions into the Sn^{4+} sites as a Cu^{2+} ion has an ion radius of 0.73 Å, to be compared to 0.71 Å of a Sn^{4+} ion.

Figure 3 displays the Raman vibration modes of undoped SnO_2 and Cu-doped SnO_2 nanobelts. The peaks in the Raman spectra for the Cu-doped SnO_2 nanobelts can be divided into two groups. One group resembles the vibration modes of microcrystal SnO_2. These Raman shifts are of ~ 630, ~ 775, and ~ 477 cm^{-1}, which are consistent with the A_{1g} (symmetric Sn–O stretching), B_{2g} (asymmetric Sn–O stretching), and E_g (translational) vibration modes of SnO_2, respectively [23–25]. These peaks show that the Cu-doped SnO_2 nanobelts possess the main characteristic of the tetrag-

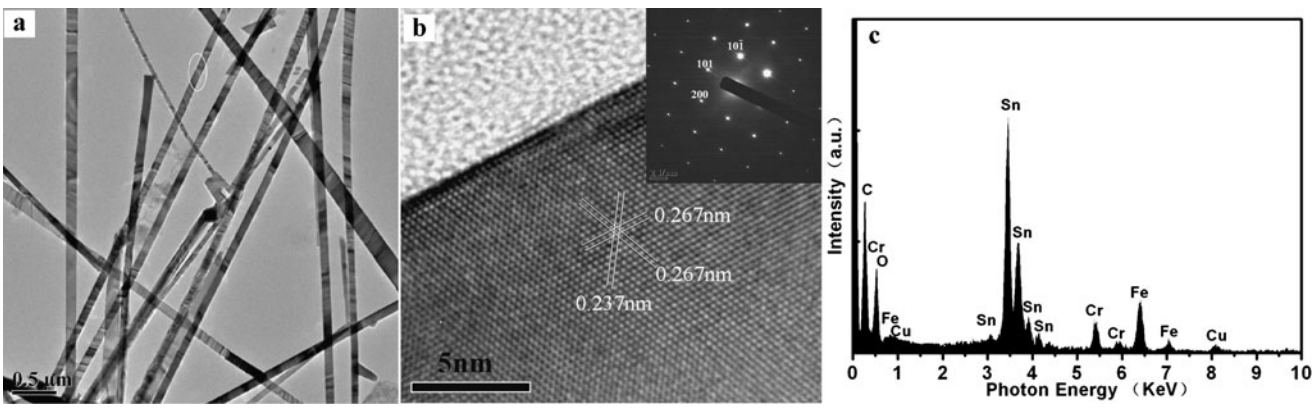

Fig. 1 (**a**) TEM image of as-fabricated Cu-doped SnO_2 nanobelts, (**b**) HRTEM image of the nanobelt indicated by the oval in (**a**), the inset is SAED pattern of the SnO_2 nanobelts. (**c**) EDS spectrum collected from the Cu-doped SnO_2 nanobelts

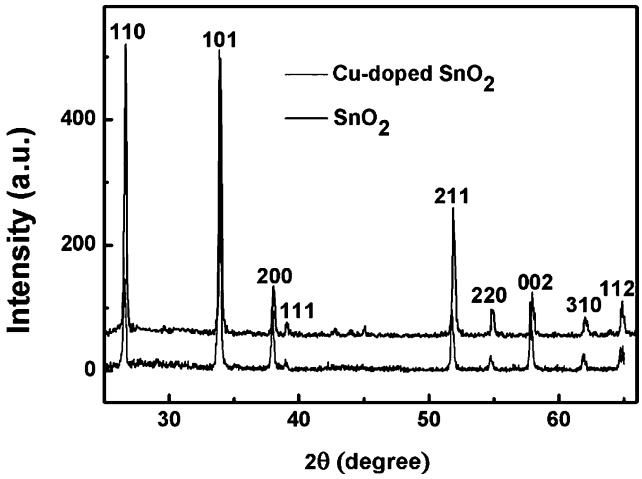

Fig. 2 XRD pattern of Cu-doped SnO_2 nanobelts and pure SnO_2 nanobelts

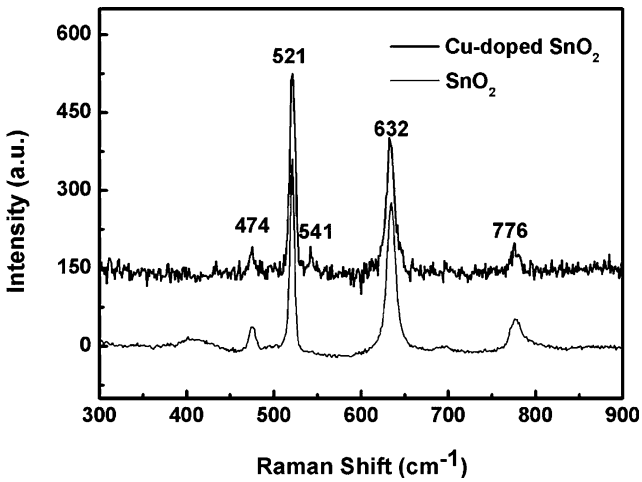

Fig. 3 Raman shift spectra of Cu-doped SnO_2 nanobelts and pure SnO_2 nanobelts

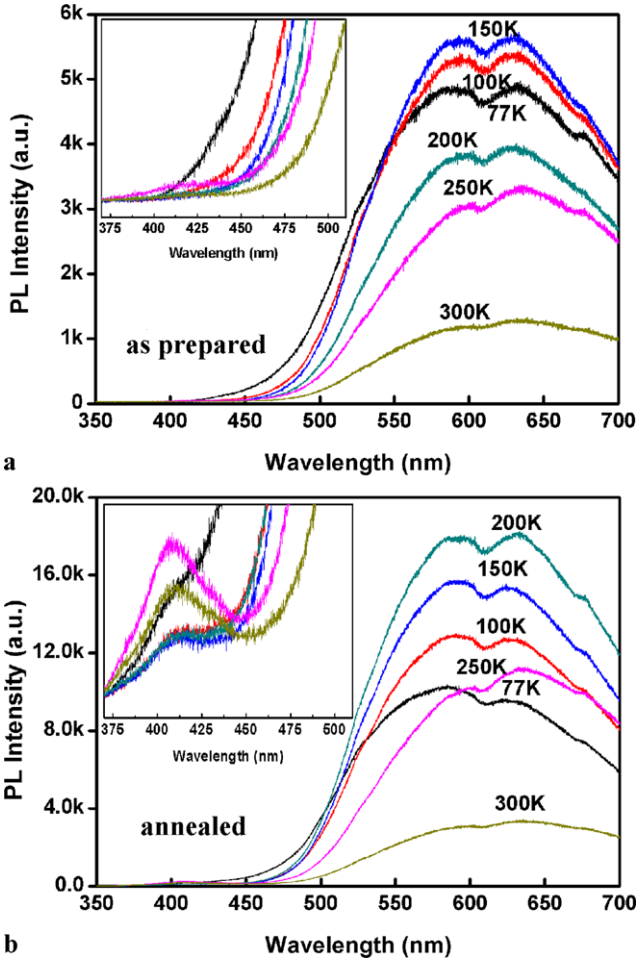

Fig. 4 Temperature dependence of the PL spectra of as-prepared (**a**) and annealed (**b**) Cu-doped SnO_2 nanobelts. Insets are their corresponding amplifying images in 370–500 nm parts

onal rutile structure. It was also found that the symmetric A_{1g} (~632 cm^{-1}) mode peak position of Cu doped in SnO_2 weakly shifted toward lower frequency. For Cu-doped SnO_2 samples, we have also revealed another group of the Raman shifts at ~541 cm^{-1}. The peak observed at ~541 cm^{-1} is believed to be an additional feature in the rutile structure. It is identified to be of S_2 mode, which is suggested to be the consequence of the disorder activation of SnO_2 nanostructures [26]. And such vibrations may be related to the Cu^{2+} ions accompanied by O vacancy. The possible mechanism of incorporation of Cu into the SnO_2 lattice can be proposed as the substitution of Sn^{4+} by Cu^{2+} ions. Finally, the peak at 521 cm^{-1} is originating with Si substrates.

Figure 4 shows the temperature dependence of the photoluminescence (PL) spectra measured from 350 to 700 nm using a 325 nm He–Cd laser. The as-prepared Cu-doped SnO_2 nanobelts exhibit different luminescence bands at different temperatures (Fig. 4(a)). At temperatures below 150 K, the nanobelts show two symmetric, smooth, and broad luminescence band centered at around 590 nm (2.1 eV) and 630 nm (1.96 eV), with a right shoulder at 677 nm (1.83 eV), whereas at higher temperatures, the asymmetric broad luminescence band centered at about 630 nm with a left shoulder at 590 nm and a right shoulder at 677 nm was observed. The intensity of the peaks increases slightly from 77 to 150 K and then decreases with increasing temperature. The temperature has an obvious influence on the competition of the emission band at 590 nm and 630 nm. The inset of Fig. 4(a) shows the amplifying images in 370–500 nm parts and no peaks was observed. In the undoped SnO_2, the PL spectra exhibit broad emission centered at about 585 nm and 620 nm [27], but without any luminescence peak around 677 nm, so we concluded that the emission centered at 677 nm is originating with Cu ions.

Figure 4(b) displays the low-temperature PL result of the sample annealed in oxygen at 800°C. This sample shows a PL spectrum that is different to that obtained from the as-

prepared sample. There are two luminescence bands centered at 590 nm and 630 nm, and a right shoulder at 677 nm, but the intensity of the sample annealed in oxygen is higher by more than three times. A slightly red shifted was observed by the temperature increasing and the competition of emission band at 590 nm and 630 nm was also appeared. The intensity of the peaks increases from 77 to 200 K and then decreases with increasing temperature. When the temperature is higher than 100 K, the near band edge of the luminescence band centered at 400 nm appears (shown in the inset of Fig. 4(b)).

Since the band gap of the present SnO_2 nanobelts is 3.6–4.2 eV (295–344 nm) as determined by UV/visible absorption, all the observed luminescence bands cannot be ascribed to the direct recombination of a conduction electron in the Sn 4d band with a hole in the O 2p valence band. The introduction of Cu ions could create a series of defects in the SnO_2 host. Such defects (e.g., dislocations and oxygen vacancies) might supply proper location sites and act as the sensitizer for the energy transfer to Cu ions due to the strong mixing of charge transfer states, resulting in the luminescence. The luminescence band at 400 nm observed from the sample annealed in oxygen maybe originates from decrease of the surface oxygen deficiency. Ferromagnetism is observed in the Cu-doped SnO_2 sample [28], the PL intensity exhibits continuous suppression with decreasing temperature, it may be attributed to the magnetic ordering induced spin sensitive energy transfer below ferromagnetic transition temperature [29].

Field-emission properties of the samples were measured by using a simple diode configuration in a vacuum chamber under a pressure of 1×10^{-5} Pa. The Si substrate covered by Cu-doped SnO_2 nanobelts (as a cathode) was separated from an indium tin oxide (ITO)/glass anode by two Teflon spacers with a thickness of 200 μm. The measured emission area was about 1 cm^2. Figure 5 plots the FE current density as a function of the applied electric field for the samples. It is visible that the Cu-doped nanobelts possess good FE properties with a turn-on field (defined as the field where the current density reaches 0.1 mA cm^{-2}) of ~2.9 V μm^{-1} and a threshold field (defined as the field where the current density reaches 1 mA cm^{-2}) of ~4.8 V μm^{-1}. The threshold field of undoped SnO_2 nanowires is about 6.5 V μm^{-1}, and that of undoped SnO_2 zigzag nanobelts is about 5.1 V μm^{-1} [27].

To further analyze the emission properties of the nanostructures, the F-N law was employed to describe the exponential dependence between the emission current and the applied field. It can be expressed as:

$$J = AF^2/\phi \exp\left(-B\Phi^{3/2}/F\right) \tag{1}$$

where A and B are constants with the values of 1.5×10^{-6} ($A{\cdot}eV{\cdot}cm^2{\cdot}V^{-2}$) and 6.8×10^7 ($V{\cdot}eV^{-3/2}{\cdot}cm^{-1}$), J is the electron current density, F is the local electric field, β is the field enhancement factor, and Φ is the work function of the emitter. For an isolated model:

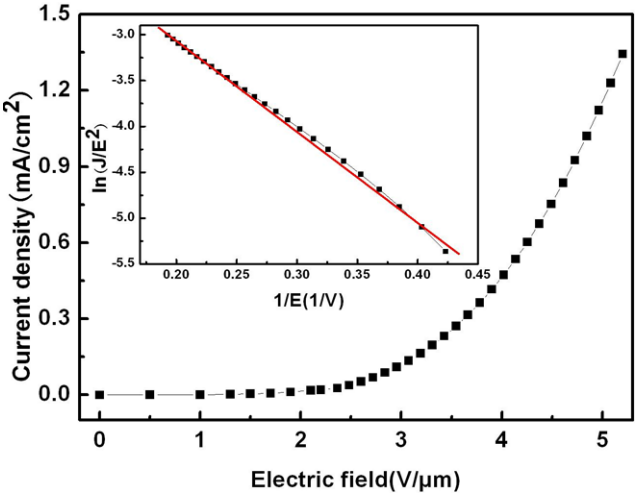

Fig. 5 FE current density versus electric field (J–E) for Cu-doped SnO_2 nanobelts showing a turn-on field of ~2.9 V/μm and a threshold field of ~4.8 V/μm. The inset is the corresponding FN plot

$$F = \beta V/d \tag{2}$$

Here V is the applied voltage, d is the distance between the anode and the cathode, and is the F-N enhancement factor. Combining with expressions (1) and (2), we obtain:

$$\ln\left(I/V^2\right) = 1/V\left(-6.8 \times 10^7 d\phi^{3/2}/\beta\right) + \text{offset} \tag{3}$$

So the $\ln(I/V^2)$ should have a linear relationship with $(1/V)$, where I is the field-emission current. The inset of Fig. 5 corresponds to the F-N plots of the Cu-doped SnO_2 nanobelts, showing that the field mission behaviors from the measured samples can be well described by the F-N law. Therefore, the as-fabricated Cu-doped SnO_2 nanobelts offer a promising candidate in future device applications such as flat panel displays and high brightness electron sources.

4 Conclusion

In summary, the single-crystalline Cu-doped SnO_2 nanobelts were synthesized by using a thermal evaporation and condensation method on silicon substrate. The temperature dependence photoluminescence characteristics of the as-prepared and annealed Cu-doped SnO_2 nanobelts have been studied in detail. Two luminescence bands centered at 590 nm and 630 nm, and a right shoulder at 677 nm were observed in both samples. And a luminescence band at 400 nm observed from the sample annealed in oxygen maybe originates from the decrease of surface oxygen deficiency. Field-emission measurements of the sample demonstrated that the nanobelts possessed excellent field-emission performance,

which provides us with a promising future for using Cu-doped SnO_2 structures as a competitive cathode material in field-emission microelectronic devices.

Acknowledgements The authors acknowledge the financial support from the Chinese National Key Basic Research Special Found (Grant Nos. 2006CB921704 and 2007CB924902), the NSF of China (Grant Nos. 60976014 and 60976004), the Key Basic Research Project of Scientific and Technology Committee of Shanghai (Grant No. 09DJ1400202), and the Specialized Research Fund for the Doctoral Program of Higher Education (Grant No. 20070269016).

References

1. S. Iijima, Nature **354**, 56 (1991)
2. W. Han, S. Fan, Q. Li, Y. Hu, Science **277**, 1287 (1997)
3. A. Morales, M. Lieber, Science **279**, 208 (1998)
4. Z. W Pan, Z.R. Dai, Z.L. Wang, Science **291**, 1947 (2001)
5. D. Ma, C. Lee, F. Au, S. Lee, Science **299**, 1874 (2003)
6. X.Y. Kong, Y. Ding, R. Yang, Z. Wang, Science **303**, 1348 (2004)
7. A. Kolmakov, Y.X. Zhang, G.S. Cheng, M. Moskovits, Adv. Mater. **15**, 997 (2003)
8. R.D. Cakan, Y.S. Hu, M. Antonietti, J. Maier, M.M. Titirici, Chem. Mater. **20**, 1227 (2008)
9. S. Ferrere, A. Zaban, B.A. Gregg, J. Phys. Chem. B **101**, 4490 (1997)
10. Y.J. Chen, Q.H. Li, Y.X. Liang, T.H. Wang, Q. Zhao, D.P. Yu, Appl. Phys. Lett. **85**, 5682 (2004)
11. B. Geng, G. Wang, Z. Jiang, T. Xie, S. Sun, G. Meng, L. Zhang, Appl. Phys. Lett. **83**, 4791 (2003)
12. C. Ronning, P. Gao, Y. Ding, Z. Wang, D. Schwen, Appl. Phys. Lett. **84**, 783 (2004)
13. J. Jie, G. Wang, X. Han, Q. Yu, Y. Liao, G. Li, J. Hou, Chem. Phys. Lett. **387**, 466 (2004)
14. S. Brovelli, N. Chiodini, F. Meinardi, A. Lauria, A. Paleari, Appl. Phys. Lett. **89**, 153126 (2006)
15. X.T. Zhou, F. Heigl, M.W. Murphy, T.K. Sham, T. Regier, I. Coulthard, R.I.R. Blyth, Appl. Phys. Lett. **89**, 213109 (2006)
16. T. Moon, S.T. Hwang, D.R. Jung, D. Son, C. Kim, J. Kim, M. Kang, B. Park, J. Phys. Chem. C **111**, 4164 (2007)
17. D. Calestani, L. Lazzini, G. Salviati, M. Zha, Cryst. Res. Technol. **40**, 937 (2005)
18. G. Faglia, C. Batto, G. Sberveglieri, M. Zha, A. Zappettini, Appl. Phys. Lett. **86**, 011923 (2005)
19. D. Cai, Y. Su, Y. Chen, J. Jiang, Z. He, L. Chen, Mater. Lett. **59**, 1984 (2005)
20. D. Maestre, A. Cremades, J. Piqueras, J. Appl. Phys. **97**, 044316 (2005)
21. S.H. Luo, Q. Wan, W.L. Liu, M. Zhang, Z.F. Di, S.Y. Wang, Z.T. Song, C.L. Lin, J.Y. Dai, Nanotechnology **15**, 1424 (2004)
22. J.H. He, T.H. Wu, C.L. Hsin, K.M. Li, L.J. Chen, Y.L. Chueh, L.J. Chou, Z.L. Wang, Small **2**, 116 (2006)
23. X. Mathew, J.P. Enriques, C.M. Garcia, G.C. Puente, M.A.C. Jacome, J.A.T. Antonio, J. Hays, A. Punnoose, J. Appl. Phys. **100**, 073907 (2006)
24. A. Dieguez, A. Romano-Rodriguez, A. Vila, J.R. Morante, J. Appl. Phys. **90**, 1550 (2001)
25. K.N. Yu, Y. Xiong, Y. Liu, C. Xiong, Phys. Rev. B **55**, 2666 (1997)
26. J.X. Wang, D.F. Liu, X.Q. Yan, H.J. Yuan, L.J. Ci, Z.P. Zhou, Y. Gao, L. Song, L.F. Liu, W.Y. Zhou, G. Wang, S.S. Xie, Solid State Commun. **130**, 89 (2004)
27. J. Wu, K. Yu, L.J. Li, J.W. Xu, D.J. Shang, Y.E. Xu, Z.Q. Zhu, J. Phys. D: Appl. Phys. **41**, 185302 (2008)
28. L.J. Li, K. Yu, Z. Tang, Z.Q. Zhu, Q. Wan, J. Appl. Phys. **101**, 014303 (2010)
29. I. Sarkar, M.K. Sanyal, S. Takeyama, S. Kar, H. Hirayama, H. Mino, F. Komori, S. Biswas, Phys. Rev. B **79**, 054410 (2009)